Time-resolved dose evaluation in an X- and gamma-ray irradiated silver-activated glass detector for three-dimensional imaging applications

Time-resolved dose evaluation in an X- and gamma-ray irradiated silver-activated glass detector for three-dimensional imaging applications

T. Kurobori [a,*], H. Itoi [a], Y. Yanagida [b], Y. Q. Chen [c]

[a] Graduate School of Natural Science and Technology, Kanazawa University, Kanazawa 920-1192, Japan
[b] Oarai Research Center, Chiyoda Technol Corporation, Oarai 311-1313, Japan
[c] China Techwin Co., Ltd, Dongguan, Guangdong 523467, China

ABSTRACT

Ag-activated phosphate glass based on the radiophotoluminescence (RPL) phenomenon has been used as the most commonly known RPL material and as an accumulated-type passive detector. In this work, the transient-state evaluation of the dose distributions achieved by X- and gamma-ray irradiations within the Ag-activated phosphate glass was performed using a time-resolved technique for the first time. Specifically, the blue RPL intensity ascribed to the electron-trapped Ag^0 centres as a function of the depth at the vicinity of the surface was investigated for different types of radiation and a wide range of energies. In addition, the dose distributions at each layer within the glass confirmed by the time-resolved measurement were compared with those reconstructed by a disk-type transparent glass detector based on the blue RPL with a diameter of 100 mm.

Keywords: Ag-activated phosphate glass, Time-resolved spectra, 3D imaging, Radiophotoluminescence (RPL), Passive dosimeter

[*]Corresponding author. Tel.: +81-76-264-5478; fax: +81-76-234-4132.
[*] *E-mail address*: kurobori@staff.kanazawa-u.ac.jp (T. Kurobori).

1. Introduction

A commercially available silver (Ag)-activated phosphate glass dosimeter based on the radiophotoluminescence (RPL) phenomenon is a type of passive dosimeter, which is still in demand and is frequently obligatory in radiation protection, and is recognized to possess several desirable characteristics, such as non-destructive readout capability, long-term stability against fading, a wide dynamic range and uniformity/batch homogeneity [1-3].

The basic principles for acquiring the doses and/or images using Ag-activated phosphate glass are as follows: before exposure, the Ag-activated phosphate glass consists of a substrate that contains positively charged silver ions (Ag^{+}) and negatively charged phosphate (PO_4^{3-}) ions. After exposure, the radiation-induced Ag-related species, mainly electron-trapped (Ag^{0}) and hole-trapped (Ag^{2+}) silver centres are produced within the glass. By optical pumping in the ultraviolet (UV) light, the Ag^{0} and Ag^{2+} centres emit an intense blue and orange luminescence, respectively. This phenomenon is generally known as RPL [4]. As the RPL intensity is proportional to the amount of the irradiation received; therefore, it is suitable for long term personal dose monitor or environmental radiation monitor. Heating to 360 ºC for 10 min following readout of the doses and/or images allows the detectors to be reused.

Other passive dosimeters based on the optically stimulated luminescence (OSL) [5], thermoluminescence (TL) [6] and photoluminescence (PL) [7] phenomena have been widely used for personal and clinical dosimetry and also used as a tool for micro radiography [8], proton beam diagnostics [9], heavy charged particle spectroscopy [10] and radionuclide imaging spectroscopy [11]. Although these types of passive luminescent dosimeters have each advantages and disadvantages, however, there have been a few detectors capable of

accumulating three-dimensional (3D) images over large areas and reconstructing dose distributions within several minutes.

Recently, we proposed and demonstrated a novel disk-type two-dimensional (2D) imaging detector with the aforementioned superior characteristics of Ag-activated RPL glass for the first time [12]. In addition, we performed a comparative investigation of the 2D dose images acquired using Ag-activated phosphate glass based on the orange RPL of atomic-scale Ag-related species and those acquired using LiF thin films based on the PL of the F-aggregate colour centres (CCs). In addition, we evaluated the performances of the two detectors [13, 14].

In this paper, the transient-state evaluation of dose distributions in an Ag-activated phosphate glass detector via a time-resolved spectral technique is presented for the first time to evaluate and understand accurate 3D dose imaging. Specifically, the intensity in Ag-activated glass based on the blue and orange RPL as a function of the depth at the vicinity of the surface within the material is investigated for different types of radiation, such as X- and gamma-rays, and a wide range of energies. In addition, it is demonstrated that the use of a confocal detection system and a transparent disk-type glass detector allows one to reconstruct the 3D dose distribution by combining images collected at different depths, which are obtained using a home-made readout system [13]. Finally, a comparative investigation between the reconstructed 3D dose distribution and aforementioned time-resolved dose distribution taken as a function of the depth within the sample is demonstrated.

2. Experimental procedure

2.1. Ag-activated phosphate glass

A commercially available Ag-activated phosphate glass plate was used for the optical and imaging measurements. Although the weight composition of the material used in this study was the same as that of FD-7 (Asahi Techno Glass Co., Ltd.), i.e., 31.55% P, 51.16% O, 6.12% Al, 11.00% Na and 0.17% Ag, the size and shape were different. The detector was a disk-type plate with a diameter of 100 mm and a thickness of 1 mm. For all of the optical measurements, such as absorption, excitation, RPL and time-resolved spectra, the samples were cut into rectangular plates of a suitable size (approximately $10 \times 7 \times 1$ mm^3) from the original glass dosimeter plate.

2.2. X- and γ-ray irradiations

X-ray irradiations were performed at room temperature (RT) using an X-ray unit, i.e., the voltages and current of the X-ray tube were 20, 30 and 40 kV and 10-20 mA, respectively, and the energies were 46 and 165 keV. The absorbed doses delivered to the samples ranged from 15 mGy to 3.0 Gy. Gamma irradiations were performed at RT using ^{137}Cs (662 keV) and ^{60}Co (1.17, 1.33 MeV) sources that delivered doses from 15 mGy to 1 Gy. The dose rate was calibrated using a commercially available detector. All of the samples were heated to 100 ºC for 10 min to suppress the 'build-up' kinetics after the X- and gamma-ray irradiations [4].

2.3 Steady-state optical properties

The optical absorption was determined at RT using a Hitachi U-3900H UV-Vis spectrophotometer with a 1 nm step. The RPL and excitation spectra were obtained using a Hitachi F-2500 fluorescence spectrophotometer with a 2.5 nm spectral bandwidth.

2.4 Transient-state optical properties

The time-resolved RPL spectra and decay curves for the blue and orange RPL signals were acquired using the combination of a high-repetition-rate Q-switched laser (Explorer One, Spectra Physics) at 349 nm and a multichannel analyser (PMA-12, Hamamatsu Photonics), as illustrated in Fig. 1. The pulse duration of the laser was less than 5 ns full-width at half-maximum (FWHM) at a repetition rate of 1 kHz for a pulse energy of 120 μJ in this work. The area of the beam on the glass sample through a rectangular metal slit (3×0.5 mm^2) and a cylindrical lens with a 60 mm focal length was 3×0.14 mm^2, and the fluence was 48 μJ/mm^2 (20 μJ/pulse). The time-resolved RPL spectra were measured in the wavelength range from 300 to 700 nm with a 1 ns step and a 10 ns gate time using a PMA-12 analyser equipped with an image intensifier (II). Therefore, the total temporal resolution was approximately 10 ns. The blue and orange RPL signals were acquired through a long-pass filter (#84-754, Edmund Optics) and an optical fibre. The transient-state dose distributions in the direction of the depth up to 1.0 mm within the Ag-activated phosphate glass were measured with a step of 5 μm.

3. Results and discussion

Typical time-resolved RPL spectra of the UV-laser irradiated glass after 693,000 excitation pulses for several pulse delays from -20 to 200 ns are presented in Fig. 2(a). Before UV exposure, the sample was irradiated with X-rays. The X-ray tube was operated at 30 kV and 20 mA with an absorbed dose of 3 Gy. For a delay less than a zero delay, the luminescence signal was indistinguishable from the background. After a zero delay, a broadband spectrum that peaked at 450 and 650 nm was observed. The orange RPL peaked at 650 nm and was attributed to the hole-trapped Ag^{2+} centres. There was another band that peaked at 450 nm, which is known as the blue RPL, and was attributed to the electron-trapped Ag^{0} centres [15]. Blue and orange RPL signals were simultaneously emitted at excitation wavelengths of 349 nm and 371 nm for acquiring the time-resolved spectra and 2D and 3D imaging, respectively. The characteristic excitation peaks of the blue and orange RPL signals occurred at 345 and 310 nm, respectively.

At further delays from 3 to 150 ns, the intensity of the blue RPL band rapidly decreased, whereas the intensity of the orange RPL band progressively decreased while maintaining the same spectral shape. Plotting the RPL intensity of the bands at 450 and 650 nm versus the delay time after the pulse, as shown in Fig. 2(b), revealed the luminescence decay lifetimes. The observed lifetime values were compatible with those measured previously [16] using a fluorescence lifetime spectrometer (Quantaurus-Tau C11367-14, Hamamatsu Photonics) for X-ray irradiated glasses subjected to a dose of 1 Gy, which were found to be 4.5 and 2300 ns for the blue and orange RPL signals, respectively. Here, ‘delay 0’ represents the value of a delay for which the intensity of the luminescence emitted from a sample is a temporal maximum.

The typical steady-state optical absorption spectra in Ag-activated phosphate glass with a thickness of 1.0 mm before and after X-ray irradiation are shown in Fig. 3(a). The

irradiation was operated at different X-ray conditions; i.e., the voltages and current of the X-ray tube were 20, 30 and 40 kV and 10 mA, respectively. The absorption spectra were attributed to the superposition of a number of individual absorption bands that corresponded to the atomic Ag atoms, charged Ag-aggregate CCs, neutral Ag molecular clusters, and phosphorous- and oxygen-related species in the range from 250 to 700 nm, as reported previously [17]. In addition, the RPL spectra excited at 350 nm for the same sample after each X-ray irradiation are shown in the inset of Fig. 3(a). This figure illustrates that the total RPL intensity, i.e., the total integrated areas of the bands between 350 and 700 nm, was nearly proportional to the square of the tube voltage.

A set of the time-resolved RPL spectra over 80 curves at different depths with a step of 5 μm from -100 to 300 μm within the sample under X-ray irradiation are shown in Fig. 3(b). The X-ray tube was operated at 40 kV and 10 mA. Each RPL spectrum for a zero delay excited at 349 nm laser pulses was piled up, as shown in the figure. The broken lines indicate the peak wavelengths at 450 and 650 nm.

The RPL spectra corresponding to the transient-state time scale were completely different from those corresponding to the steady-state time scale presented in the inset of Fig. 3(a). The reasons are as follows: as shown in Fig. 2(b), the decay time of the blue RPL is much shorter than that of the orange RPL. The Ag^0 and Ag^{2+} CCs emitting the blue and orange RPL in Ag-activated phosphate glass will never disappear unless the glasses are annealed at a high temperature of about 400 °C [18]. Therefore, under the steady-state time scale the integrated orange RPL intensity with the long decay lifetime is enhanced in comparison with the integrated blue RPL intensity with the short decay lifetime. In addition, note that the peak wavelength for the orange RPL spectrum was markedly shifted to a longer

wavelength, from 570 (steady-state) to 650 nm (transient-state), upon UV-nanosecond-laser excitation.

Plotting the intensity of the bands that peaked at 450 and 650 nm versus the depth (distance from the surface) within the glass from -100 to 300 μm, as shown in Fig. 3(c), revealed the dose distributions for various X-ray irradiations; the voltages and current of the X-ray tube were 20, 30 and 40 kV and 10 mA, respectively. The blue and orange RPL intensities from each layer at different depths were considered to correspond to the concentration of the radiation-induced Ag^0 and Ag^{2+} CCs in the sample.

As already noted [16], we estimated the values of the absorption coefficient and re-absorption rate when light at 650 nm propagated a 500-μm length in the X-ray-irradiated glass under an absorbed dose of 1 Gy. The values were 1.15×10^{-5} (μm^{-1}) and 0.57 %, respectively. For an excitation wavelength at 371 nm, each value of the absorption coefficient and absorption rate was 1.28×10^{-4} (μm^{-1}) and 6.4 %, respectively. In order to evaluate accurate volumetric dose distributions at each layer within the glass, one must also take these values into consideration.

Figure 3(c) illustrates that the FWHM of the radiation-induced defect layer formed within the glass was approximately 70 μm for the blue RPL signal, for which the X-ray tube was operated at 40 kV and 10 mA. The background noise of the blue and orange RPL measured for the non-irradiated sample was subtracted from each RPL signal of the irradiated samples. Note that each peak of the blue RPL intensity was located in the vicinity of the surface compared to that of the orange RPL intensity.

The results suggested that the electron-trapped Ag^0 and/or Ag_2^+ (reaction: $Ag^+ + Ag^0 \rightarrow Ag_2^+$) centres, which are known to emit blue RPL by UV exposure [15], might be localized at the near-surface layers within the glass because the glass surface was subjected to various

morphological damages, such as heat treatment, i.e., pre-heating and annealing in a muffle furnace at 100 °C and 360 °C for 10 min, respectively, as well as mechanical polishing in air. In addition, according to the radiation-induced effects in phosphate glass, the oxygen-related hole centres (OHCs) and phosphorus-oxygen-hole-centre (POHCs) due to one or two non-bridging oxygen atoms of a PO_4 unit trapping a hole are easily formed in the near-surface layers of glasses [19, 20]. Therefore, the Ag^+ ions introduced into the host glass were coupled to the non-bridging oxygen atoms of a PO_4 to maintain electrical neutrality, and then, the Ag^+ ions were gathered and localized in the near-surface layers. After exposure, the electron-trapped Ag^0 centres immediately formed in the nearest-surface layers within a short time, whereas the hole-trapped Ag^{2+} centres gradually formed in thick near-surface layers due to a slow build-up rate [4].

The time-resolved RPL spectra for a zero delay at different depths with a step of 5 μm from -100 to 300 μm within the sample under X-ray irradiation are shown in Fig. 4(a), for which the X-ray tube was operated at an energy of 165 keV and a dose of 25 mGy. Unlike the RPL spectra shown in Fig. 3(b), the blue RPL intensity peaking at 430 nm became predominant and considerably higher than that of the orange RPL intensity. The comparative RPL intensities as a function of the depth under two different X-ray energies (46 and 165 keV) with a dose of 25 mGy are shown in Fig. 4(b). Plotting the intensity of the bands that peaked at 430 nm versus the depth from -100 to 300 μm revealed the dose distributions within the sample. High-energy X-ray irradiation resulted mainly in the formation of electron-trapped Ag^0 centres.

The time-resolved RPL spectra for a zero delay at different depths with a step of 5 μm from -100 to 300 μm under ^{137}Cs (662 keV) and ^{60}Co (1.7 and 1.33 MeV) gamma-ray irradiations with a dose of 1 Gy are shown in Figs. 5(a) and 5(b), respectively. Unlike the X-

ray irradiated RPL spectra shown in Figs. 3(b) and 4(a), another band peak at 550 nm was observed in the case of the ^{137}Cs source instead of the orange band at 650 nm. The decay measurement indicated that the lifetime value of the 550 nm band consisted of fast and slow components, i.e., the values were compatible with the blue (4.5 ns) and orange (2300 ns) RPL. The comparative RPL intensity as a function of the depth for a zero delay under two different gamma-rays is shown in Fig. 5(c). The RPL intensity for gamma-ray irradiation with a dose of 1 Gy was nearly the same as the intensity for X-ray irradiation with a dose of 25 mGy for energies of 46 and 165 keV, as shown in Fig. 4(b).

A photographic image of the mask used ("Hassam House" in Kobe) is shown in Fig. 6(a). The glass detector was irradiated with soft X-rays passing through this stainless steel mask, which was 250 μm thick, and was attached to the detector with a diameter of 100 mm and a thickness of 1 mm. A series of 2D reconstructed dose distributions obtained using a disk-type Ag-activated glass plate based on the blue RPL after X-ray irradiation are shown in Figs. 6(b)-(d), for which the X-ray tube was operated at 30 kV and 10 mA with a dose of 1 Gy. A detailed description of the 2D and 3D readout system and measuring procedure for the disk-type RPL glass plate has been published elsewhere [13, 16]. The use of a confocal detection system and an objective lens with a numerical aperture (NA) of 0.90 and a working distance of 1 mm enabled the reconstruction of the 3D dose distributions that were recorded within the transparent glass, which was rotated at a rate of 2400 rpm, by combining the images acquired at different depths, i.e., Figs. 6(b) near the surface, 6(c) 100 μm and 6(d) 300 μm below the surface. Such a series of the 2D dose distributions from the X-ray irradiated glass were compared with the time-resolved dose distributions taken as a function of the depth, as shown in Fig. 3(c), for which the X-ray tube was operated at 30 kV and 10

mA. The reconstructed blue RPL dose distributions, as shown in Figs. 6(b)-(d), rapidly decreased at the depth of approximately 100 μm from the surface.

However, in order to obtain a 3D dose imaging, it should be necessary to calibrate or compare the measured depth distribution of active luminescent centers, as shown in Figs. 6(b)-(d) and Fig. 3(c), with the deposited energy curves of the used X- and gamma-rays in the sample depth.

Very recently, the proton irradiation of LiF bulk and thin films was simulated [9] by using the SRIM (The Stopping and Range of Ions in Matter) software package. If the SRIM and other software such as the Monte Carlo (MC) simulations based on the GEANT4 [21, 22] are available for our system, the energy loss can be calculated as a function of the implantation depth in the Ag-activated phosphate glass for various values of the X- and gamma-ray energies. Now the subject is under consideration.

4. Conclusion

The data obtained in this study led to the following conclusions:

(1) The steady- and transient-state optical properties of the blue and orange RPL of Ag-activated phosphate glass, including the time-resolved spectra and nanosecond-time-scale decay curves, were compared.

(2) The blue and orange RPL intensities as a function of the depth from the surface were measured, and the dose distributions and their radiative characteristics were demonstrated and discussed for different types of radiation and a wide range of energies.

(3) The origin and mechanism for the intensity enhancement of the blue RPL in the near-surface layers were qualitatively discussed for the X-ray-irradiated Ag-activated glass.

(4) A comparative investigation between the time-resolved dose distributions taken as a function of the depth within the glass and the 3D dose distributions based on the blue RPL reconstructed from the use of a home-made readout system was performed for the X-ray-irradiated Ag-activated glass.

The investigated Ag-activated phosphate glass detector, based on the blue and orange RPL phenomenon, exhibits superior characteristics and should be suitable for microradiography, X-ray microscopy, radiation diagnostics, fluorescent nuclear track detection as well as in outdoor environments, e.g., in structural health monitoring for buildings, tunnels and bridges.

Acknowledgements

T. K would like to thank Prof. H. Nanto at the Kanazawa Institute of Technology for valuable discussions and thank Mr. Y. Koguchi and Mr. N. Takeuchi at Chiyoda Technol Corporation for their contributions to the sample preparation. This work was supported by JSPS, a Grant-in-Aid for Scientific Research (B), No. 26289362 and partially by JST A-step, No. AS251Z01722P and AS262Z00986P.

References

[1] R. Yokota, H. Imagawa, Journal of the Physical Society of Japan 23 (5) (1966) 1038.

[2] S-M. Hsu, S-H. Yeh, M-S. Lin, W-L. Chen, Radiation Protection Dosimetry 119 (1-4) (2006) 327.

[3] T. Yamamoto, D. Maki, F. Sato, Y. Miyamoto, H. Nanto, T. Iida, Radiation Measurements 46 (12) (2011) 1554.

[4] J. A. Perry, RPL Dosimetry, Radiophotoluminescence in Health Physics. Taylor & Francis, New York (1987) Chapters 1 and 4.

[5] E. G. Yukihara, S. W. S. McKeever, Optically Stimulated Luminescence. John Wiley & Sons, New York (2011) p.278.

[6] P. Olko, B. Marczewska, L. Czopyk, M. A. Czermak, M. Kłosowski, M. P. R. Waligórski, Radiation Protection Dosimetry 118 (2) (2006) 213.

[7] G. Baldacchini, E. de Nicola, R. M. Montereali, A. Scacco, V. Kalinov, Journal of Physics and Chemistry of Solids 61 (1) (2002) 21.

[8] G. Baldacchini, F. Bonfigli, A. Faenov, F. Flora, R. M. Montereali, A. Pace, T. Pikuz, L. Reale, Journal of Nanoscience and Nanotechnology 3 (6) (2003) 483.

[9] M. Piccinini, F. Ambrosini, A. Ampollini, M. Carpanese, L. Picardi, C. Ronsivalle, F. Bonfigli, S. Libera, M. A. Vincenti, R. M. Montereali, Journal of Luminescence, 156 (11) (2014) 170.

[10] G. M. Akselrod, M. S. Akselrod, E. R. Benton, N. Yasuda, Nuclear Instruments and Methods in Physics Research B 247 (2) (2006) 295.

[11] J. A. Bartz, C. J. Zeissler, V. V. Fomenko, M. S. Akselrod, Radiation Measurements, 56 (9) (2013) 273.

[12] T. Kurobori, S. Nakamura, Radiation Measurements 47 (10) (2012) 1009.

[13] T. Kurobori, Y. Miyamoto, Y. Maruyama, T. Yamamoto, T. Sasaki, Nuclear Instruments and Methods in Physics Research B 326 (5) (2014) 76.

[14] T. Kurobori, A. Matoba, Japanese Journal of Applied Physics 53 (02BD14) (2014) 1.

[15] T. Kurobori, W. Zheng, Y. Miyamoto, H. Nanto, T. Yamamoto, Optical Materials 32 (9) (2010) 1231.

[16] T. Kurobori, Y. Maruyama, Y. Miyamoto, T. Sasaki, T. Yamamoto, 12th Europhysical Conference of Defects in Insulating Materials (Eurodim 2014), Canterbury, UK, #No.1.

[17] W. Zheng, T. Kurobori, Journal of Luminescence 131 (1) (2011) 36.

[18] Y. Miyamoto, H. Nanto, T. Kurobori, Y. Fujimoto, T. Yanagida, J. Ueda, S. Tanabe, T. Yamamoto, Radiation Measurements 71 (12) (2014) 529.

[19] P. Ebeling, D. Ehrt, M. Friedrich, Optical Materials 20 (2) (2002) 101.

[20] D. L. Griscom, E. J. Friebele, K. J. Long, J. W. Fleming, Journal Applied Physics 54 (7) (1983) 3743.

[21] S. Agostinelli et al., Nuclear Instruments and Methods in Physics Research A, 506 (3) (2003) 250.

[22] G. O. Sawakuchi et al., Medical Physics, 37 (9) (2010) 4960.

Figure Captions:

Fig. 1. Acquisition setup for the measurement of the time-resolved RPL spectra and decay curves of the X-ray-irradiated Ag-activated phosphate glass. A laser beam with a rectangular beam shape was incident on a side facet of the sample. The grey arrow indicates the sample movement direction.

Fig. 2. (a) Time-resolved RPL spectra of X-ray-irradiated Ag-activated glass after UV laser irradiation at 349 nm for several pulse delays. (b) Luminescent decay curves of X-ray-irradiated Ag-activated glass acquired at 450 and 650 nm for the blue and orange RPL, respectively.

Fig. 3. (a) Steady-state absorption spectra in Ag-activated glass before and after X-ray irradiation and the corresponding RPL spectra excited at 350 nm shown in the inset. (b) A set of time-resolved RPL spectra at different depths within the sample under X-ray irradiation at 40 kV and 10 mA. (c) Plot of the intensity of the blue (at 450 nm) and orange (at 650 nm) RPL vs. the depth from the surface under different X-ray conditions: 20, 30 and 40 kV and 10 mA.

Fig. 4. (a) A set of time-resolved RPL spectra at different depths within the sample under an energy of 165 keV with a dose of 25 mGy. (b) Plot of the intensity of the blue RPL at 430 nm vs. the depth from the surface under different energies: 46 and 165 keV.

Fig. 5. (a) A set of time-resolved RPL spectra at different depths within the sample under ^{137}Cs gamma-ray irradiation with a dose of 1 Gy. (b) A set of time-resolved RPL spectra at different depths within the sample under ^{60}Co gamma-ray irradiation with a dose of 1 Gy. (c) Plot of the intensity of the blue (at 430 nm), green (at 550 nm) and orange (at 650 nm) RPL vs. the depth from the surface under ^{137}Cs and ^{60}Co gamma-ray irradiation with a dose of 1 Gy.

Fig. 6. (a) Photographic image of the mask used for X-ray irradiation under the conditions of 30 kV and 10 mA with a dose of 1 Gy. A set of reconstructed dose distributions for each image at different depths: (b) the vicinity of the surface, (c) 100 and (d) 300 μm below the surface.

1.0-column

Fig. 1 T. Kurobori

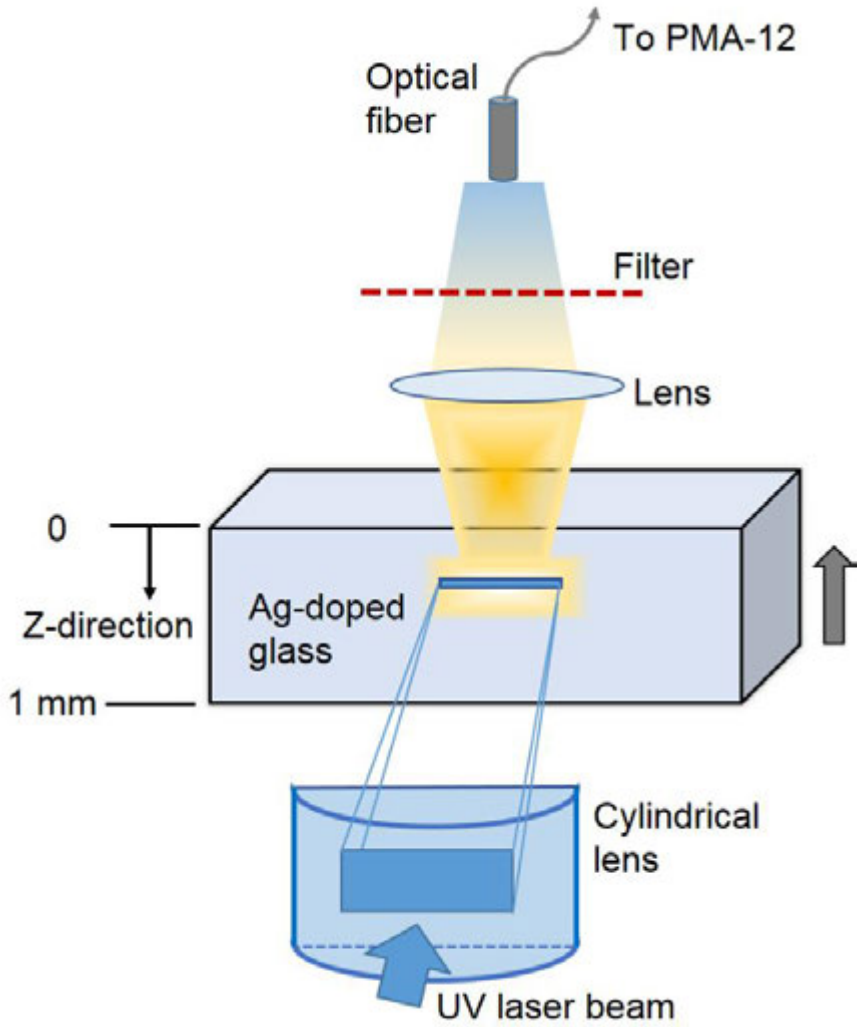

1.0-column

Fig. 2　T. Kurobori

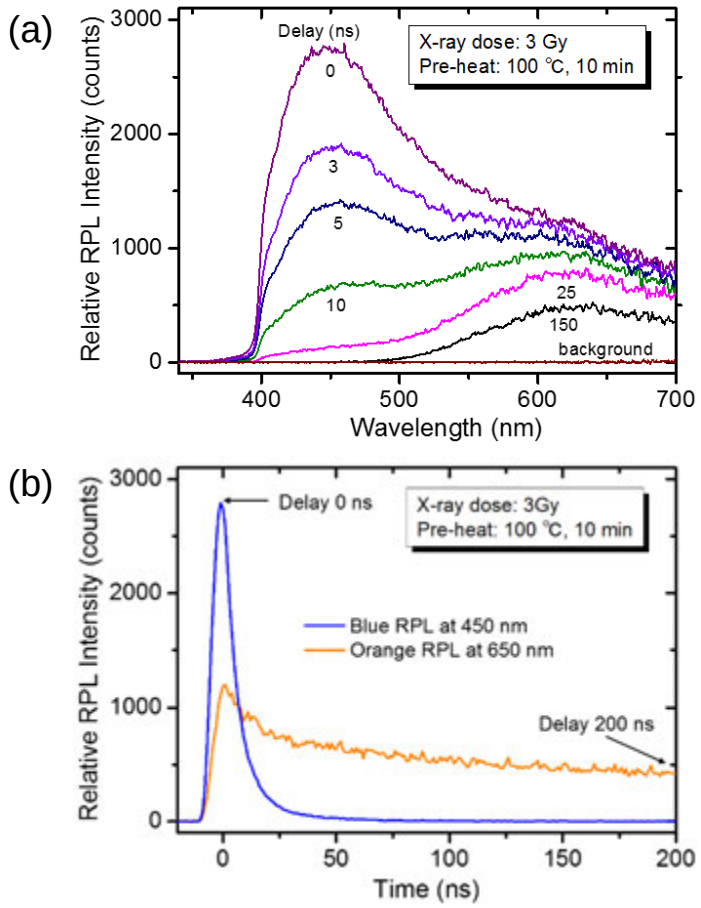

1.0-column

Fig. 3 T. Kurobori

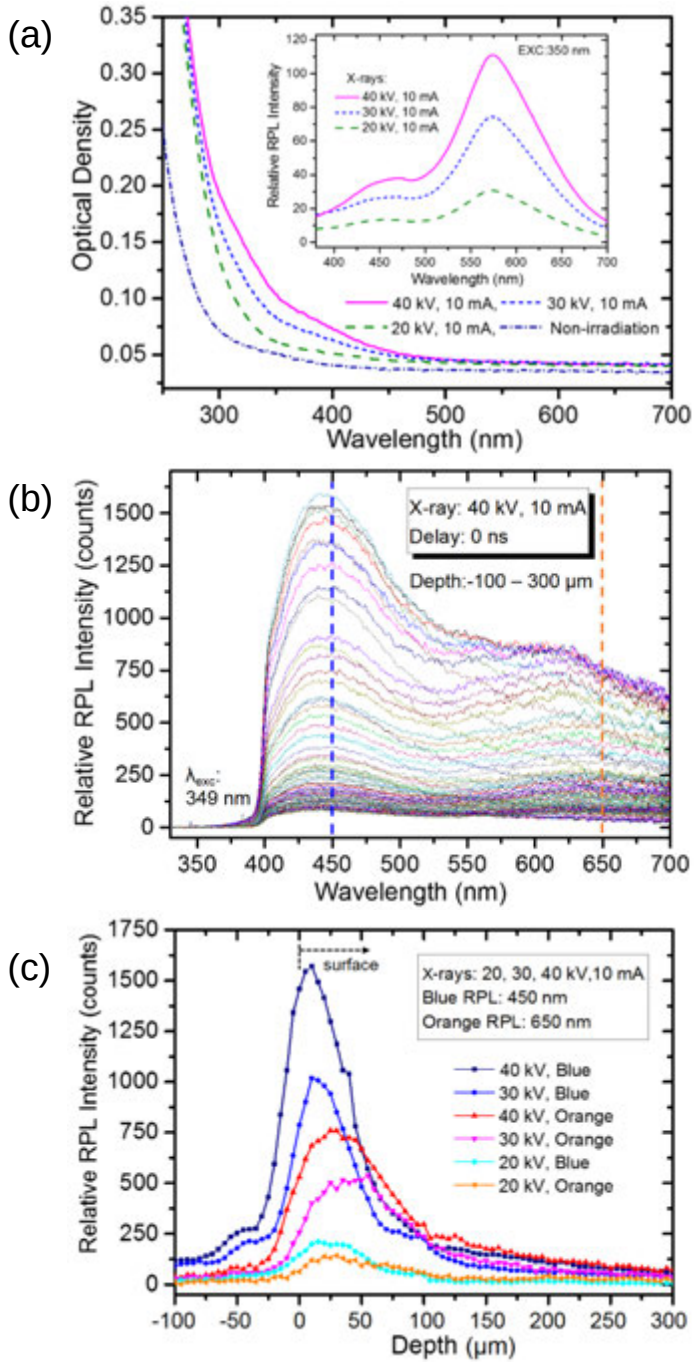

1.0-column

Fig. 4　T. Kurobori

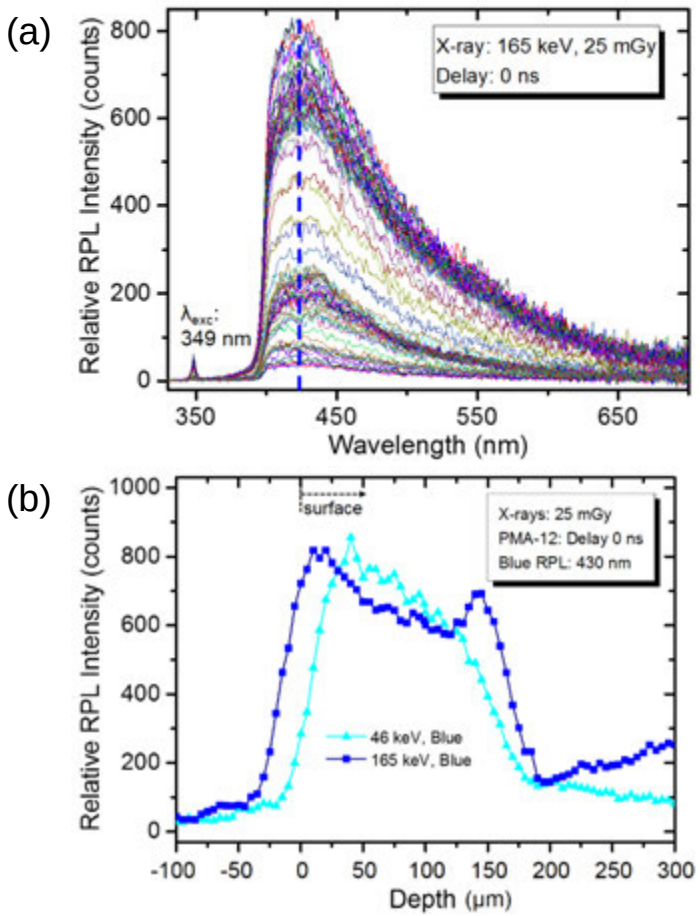

1.0-column

Fig. 5 T. Kurobori

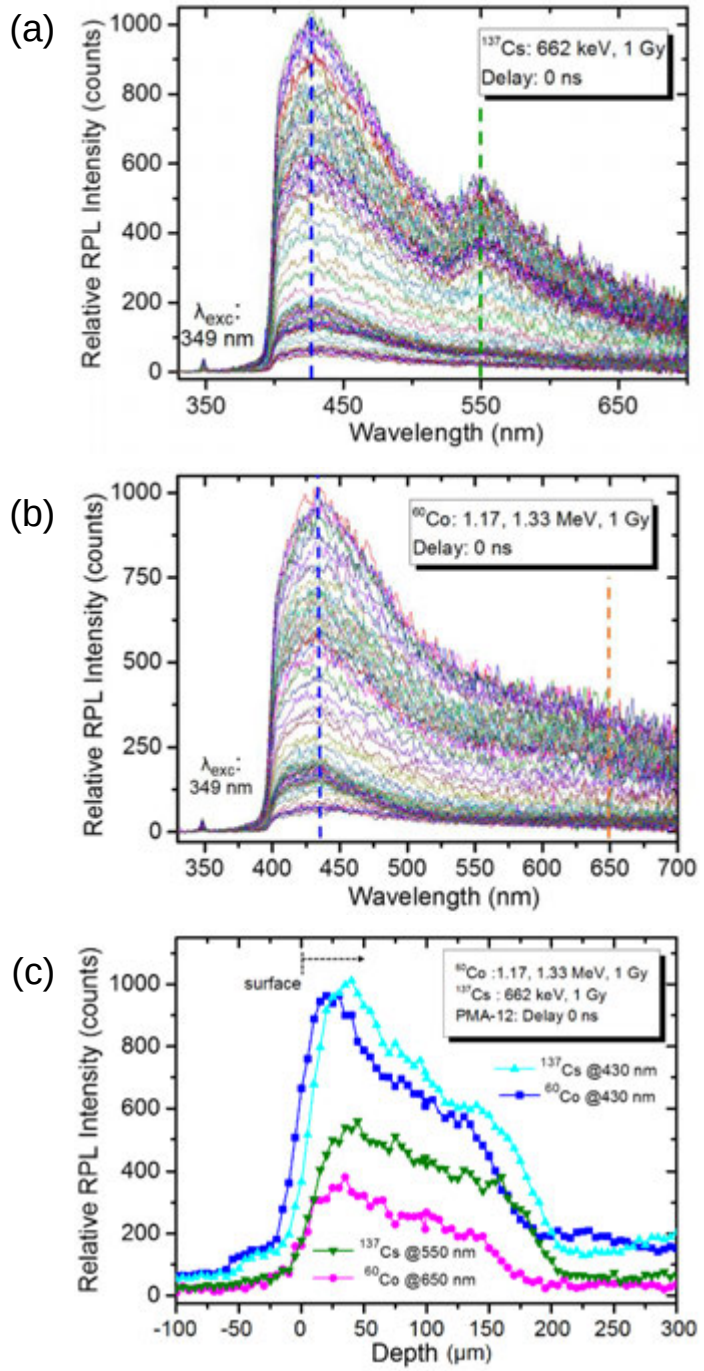

1.5-column

Fig. 6　T. Kurobori